Chapter 2
Historical Development of Constitutive Relations for Addressing Subsurface LNAPL Contamination

Robert J. Lenhard and Jonás García-Rincón

Abstract An overview of the historical development of *k-S-P* relations (constitutive relations) to model potential flow of light nonaqueous phase liquids (LNAPLs) in the subsurface is presented in this chapter. The focus is advancements proposed by Parker, Lenhard, and colleagues over time. Discussion includes constitutive relations for incorporation in numerical multiphase flow models as well as constitutive relations for predicting subsurface LNAPL volumes and transmissivities from fluid levels measured in monitoring groundwater wells. LNAPL saturation distributions are given for various subsurface properties and layering sequences.

Keywords Capillary pressure · LNAPL saturation · LNAPL-specific volume · Multiphase modeling · Relative permeability

2.1 Introduction

The potential contamination of groundwater by hydrocarbon fuels, such as gasoline (petrol), diesel, and heating oils, has existed since these products were produced. Hydrocarbon fuels, which exist as light nonaqueous phase liquids (LNAPLs), enter the subsurface by leaks in storage containers, pipes, and spills. Once in the subsurface, hydrocarbon compounds can potentially partition in water and contaminate groundwater resources. Typically, hydrocarbon fuels consist of many compounds each with different capabilities (properties) for partitioning into water, subsurface gas, and onto solid matter. Groundwater becomes contaminated by (1) dissolved fuel compounds moving downward by gravity in the vadose zone as water recharges the surface aquifer; (2) volatized fuel compounds partitioning in vadose zone water and

R. J. Lenhard (✉)
San Antonio, TX, USA
e-mail: rj.lenhard@yahoo.com

J. García-Rincón
Legion Drilling and Numac, 11–13 Metters Place, Wetherill Park, NSW 2164, Australia

J. García-Rincón et al. (eds.), *Advances in the Characterisation and Remediation of Sites Contaminated with Petroleum Hydrocarbons*, Environmental Contamination Remediation and Management, https://doi.org/10.1007/978-3-031-34447-3_2

groundwater; and (3) direct partitioning into groundwater as the fuels collect at the top of the water-saturated region or get entrapped in it. In this chapter, we briefly discuss the efforts to model subsurface LNAPL behavior including permeability (k)-saturation (S)-pressure (P) relations; prediction of subsurface LNAPL saturations, volumes, and transmissivities based on LNAPL and water levels in nearby groundwater wells; and conclude with suggestions for some improvements in LNAPL predictive models. A focus is on constitutive (k-S-P) relations developed by Parker, Lenhard, and colleagues.

2.2 Recognition of Health Effects from LNAPLs in the Subsurface

Initially, there was little concern of health effects from LNAPLs in the subsurface because the health effects from exposure to some of the compounds were not well understood, except for introduced alkyl leads, e.g., tetraethyl lead in the 1920s (Lewis 1985; Oudijk 2007). Lead was known to have adverse human health effects for some time. Only after relatively high occurrences of sickness and cancer were reported, the health effects from exposure to LNAPL compounds became better understood. For example, benzene, toluene, and xylenes, which are components of LNAPLs, were eventually recognized as either toxic or carcinogenic to humans (IARC 1987; ATSDR 1995; EPA 2007). As the health effects from compounds in LNAPLs were better understood, more stringent regulations were introduced to minimize potential soil and groundwater contamination. Additionally, there were requirements to clean up contaminated sites to minimize the adverse health effects to humans, limit risks to the environment, and reduce other negative impacts from subsurface LNAPL contamination.

2.3 Predicting Subsurface LNAPL Behavior: Early Developments

To plan the remediation of LNAPL-contaminated sites, cost-effective approaches and designs are needed. Practitioners need to know the volume and distribution of LNAPL in the subsurface. Initially, the thickness of LNAPL in boreholes (groundwater wells) was used to estimate the LNAPL thickness in the subsurface (de Pastrovich et al. 1979; Hall et al. 1984). The LNAPL thickness in the subsurface was then used to calculate the subsurface LNAPL-specific volume (LNAPL volume per horizontal surface area), which is an important factor for designing remediation systems. Hampton and Miller (1988) conducted laboratory investigations of the relationship between the LNAPL thickness in a borehole and that in subsurface media and concluded that the LNAPL thickness in the subsurface is not a good measurement of the LNAPL-specific volume

because other factors were involved such as porous media pore-size distributions and pore-scale physics that govern LNAPL saturation distributions. The pore-scale physics of LNAPLs in the subsurface that could potentially result in groundwater contamination, however, were well-known (van Dam 1967; Schwille 1967) when these early models were proposed. Because available computers at the time were limited, remediation practitioners used relatively simple expressions to help with remediation strategies and designs.

Abriola and Pinder (1985a,b) were among the first to develop a numerical model to address subsurface LNAPL contamination, which was able to solve the governing equations for multiphase (air, LNAPL, water) flow. Relatively soon afterward, several other multiphase flow numerical models were developed (e.g., Faust 1985; Osborne and Sykes 1986; Baehr and Corapcioglu 1987; Kuppusamy et al. 1987; Kaluarachchi and Parker 1989). To predict the potential flow of air, LNAPL, and water in incompressible porous media, a set of governing equations is

$$\phi \frac{\partial}{\partial t}(S_a \rho_a) = \nabla \left[\frac{k k_{ra} \rho_a}{\eta_a} (\nabla P_a + \rho_a g \nabla z) \right] \tag{2.1}$$

$$\phi \frac{\partial}{\partial t}(S_o \rho_o) = \nabla \left[\frac{k k_{ro} \rho_o}{\eta_o} (\nabla P_o + \rho_o g \nabla z) \right] \tag{2.2}$$

$$\phi \frac{\partial}{\partial t}(S_w \rho_w) = \nabla \left[\frac{k k_{rw} \rho_w}{\eta_w} (\nabla P_w + \rho_w g \nabla z) \right] \tag{2.3}$$

where

ϕ is the porosity (assumed to be constant for each media type),
S_a, S_o, S_w are the air, LNAPL, and water saturations, respectively,
ρ_a, ρ_o, ρ_w are the air, LNAPL, and water mass densities, respectively,
k is the intrinsic permeability tensor,
k_{ra}, k_{ro}, k_{rw} are the air, LNAPL, and water relative permeabilities, respectively,
η_a, η_o, η_w are the air, LNAPL, and water dynamic viscosities, respectively,
P_a, P_o, P_w are the air, LNAPL, and water fluid pressures, respectively,
g is the scalar gravitational constant,
t is time, and,
z is elevation.

The equations (Eqs. 2.1–2.3) need to be solved simultaneously because the dependent saturation variable in each equation is a function of the independent pressure variable of other equations as well as the relative permeabilities. Consequently, the equations are relatively difficult to solve. Hassanizadeh and Gray (1990) proposed another approach and governing equations to describe multiphase flow based on macroscale thermodynamic theory. Their equations, which were based on fundamental laws of physics, were for only two-fluid systems, but Hassanizadeh and Gray (1990) stated that it would be straightforward to extend the theory to more than two fluids.

A simplifying assumption for solving Eqs. (2.1–2.3) can be made by assuming air to be at atmospheric pressure whenever there is interconnected air (continuous air phase). Richards (1931) made such assumption when considering water movement through soils. Under this assumption, then Eq. (2.1) can be neglected. This assumption is likely realistic for soils near the interface with the atmosphere, where air can freely move from soil pores to the atmosphere and vice versa. However deeper in the subsurface, continuous air may not be atmospheric because of time-dependent atmospheric conditions. The air pressure may vary with elevation. If there are clay or cemented layers, then there may be significant differences in the air pressures on opposite sides of the layers. Air flow has been observed at breathing boreholes which means an air pressure gradient exists. Furthermore, if vacuum extraction of LNAPL vapors is employed as a remediation option, then Eq. (2.1) is needed for any computer simulations (predictions). Employing the Richards (1931) assumption may not always be valid; it would depend on subsurface conditions and what is being simulated.

Important elements for predicting multiphase flow are the physical relations, particularly the relations describing how saturations and relative permeabilities vary as a function of the fluid pressures. Typically, the relations between fluid saturations and pressures are empirically parameterized and the parameters are utilized to predict fluid relative permeabilities. For two-fluid systems (air–water or LNAPL–water), only one set of parameters is needed. For three-fluid systems (air–LNAPL–water), there can be multiple sets of parameters.

Leverett (1941) proposed that the total-liquid saturation in multiphase systems, with gas and liquid phases, is a function of the capillary pressure at gas–liquid interfaces in which gas is the nonwetting fluid. Therefore, the total-liquid saturation (sum of water and LNAPL) would be a function of the air–LNAPL capillary pressure for air–LNAPL–water systems in porous media where water is the wetting fluid and LNAPL has intermediate wettability between air and water. From the petroleum industry, the water saturation is commonly assumed to be a function of the oil–water (LNAPL–water) capillary pressure in which water is a strongly wetting fluid. For three-fluid systems, the total-liquid saturation can be predicted from the air–LNAPL capillary pressure using one set of parameters and the water saturation can be predicted from the LNAPL–water capillary pressure using another set of parameters. Both sets of parameters need to reflect the same pore-size distribution for the predictions to be accurate and avoid numerical convergence issues as the two-fluid (air–water) system transitions into a three-fluid (air–LNAPL–water) system and vice versa.

To calculate the LNAPL saturation, the water saturation is subtracted from the total-liquid saturation. Commonly, water is assumed to be the wetting fluid, air is the nonwetting fluid, and LNAPL has intermediate wettability between water and air. Under this condition and neglecting fluid films, water will preferentially occupy the smallest pore spaces, air will occupy the largest continuous pore spaces, and LNAPL will occupy intermediate-sized pore spaces. However, this wettability sequence does not hold for all porous media or LNAPLs. In some cases, porous media can have LNAPL-wet, mixed-wet, or fractional-wet wettability instead of a strongly water-wet

wettability (Anderson 1987). The distribution of fluids within the pore spaces will be governed by the wettability. Hence, the calculation of fluids saturations as a function of capillary pressures will depend on the wettability. In the following discussions in this chapter, we assume the porous media to be strongly water wet.

2.4 The Parker et al. (1987) Nonhysteretic Model

Parker et al. (1987) proposed a parametric formulation to describe nonhysteretic *k-S-P* relations for air–LNAPL–water systems in porous media where water is the wetting fluid, LNAPL has intermediate wettability, and air is the nonwetting fluid. The formulation can be calibrated relatively easily using more readily available air–water *S-P* measurements or published parameters. The scaling approach yields closed-form expressions of *k-S-P* relations that could be employed to predict behavior in two-fluid air–water, air–LNAPL, or LNAPL–water systems, or three-fluid air–LNAPL–water systems.

For *S-P* relations, Parker et al. (1987) proposed a scaled $S^*(h^*)$ functional as

$$S^*\left(h^*\right) = \overline{S}_w^{aw}(\beta_{aw}h_{aw}) \tag{2.4}$$

$$S^*\left(h^*\right) = \overline{S}_o^{ao}(\beta_{ao}h_{ao}) \tag{2.5}$$

$$S^*\left(h^*\right) = \overline{S}_w^{ow}(\beta_{ow}h_{ow}) \tag{2.6}$$

$$S^*\left(h^*\right) = \overline{S}_w^{aow}(\beta_{ow}h_{ow}) \tag{2.7}$$

$$S^*\left(h^*\right) = \overline{S}_t^{aow}(\beta_{ao}h_{ao}) \tag{2.8}$$

where superscripts aw, ao, ow, and aow refer to air–water, air–LNAPL, LNAPL–water, and air–LNAPL–water fluid systems, respectively; β_{aw}, β_{ao}, and β_{ow} refer to air–water, air–LNAPL, and LNAPL–water scaling factors, respectively; h_{aw}, h_{ao}, h_{ow} are air–water, air–LNAPL, and LNAPL–water capillary heads, respectively [$h_{aw} = (P_a - P_w)/\rho_w g$; $h_{ao} = (P_a - P_o)/\rho_w g$; $h_{ow} = (P_o - P_w)/\rho_w g$]; and $\overline{S}_w$, $\overline{S}_o$, and $\overline{S}_t$ are the effective water, LNAPL, and total-liquid saturations, respectively, defined by

$$\overline{S}_j = \left(S_j - S_m\right)/(1 - S_m) \tag{2.9}$$

in which S_j ($j = w, o, t$) are actual saturations and S_m is the minimum or irreducible wetting fluid saturation. To mathematically describe the relations, Parker

et al. (1987) adapted the van Genuchten (1980) *S-P* equation to predict the effective saturations. However, the Brooks-Corey (1966) mathematical equation or other models for describing *S-P* relations also could be used.

The fluid pair scaling factors (β_{aw}, β_{ao}, and β_{ow}) are obtained by regressing air–LNAPL and LNAPL–water *S-P* data, if available, against air–water *S-P* data; however, obtaining such data may not be available or too time-consuming and expensive to conduct. Lenhard and Parker (1987a) overcame this issue by showing that the scaling factors can be estimated from ratios of interfacial tensions as

$$\beta_{aw} = 1 \tag{2.10}$$

$$\beta_{ao} = {}^{\sigma_{aw}}\!/_{\sigma_{ao}} \tag{2.11}$$

$$\beta_{ow} = {}^{\sigma_{aw}}\!/_{\sigma_{ow}} \tag{2.12}$$

where σ_{aw}, σ_{ao}, and σ_{ow} are air–water, air–LNAPL, and LNAPL–water interfacial tensions, respectively. By defining $\beta_{aw} = 1$, Parker et al. (1987) made the *S-P* parameters to be based on air–water *S-P* relations. This made it considerably easier to obtain parameters to describe the $S^*(h^*)$ relations because one could use available air–water *S-P* data or published air–water parameters and ratios of interfacial tensions, which are more easily measured than air–LNAPL and LNAPL–water *S-P* data. Consequently, investigators can conduct numerical simulations of multiphase flow without the need and cost for *S-P* data from different fluid systems. Enforcing

$$\beta_{aw} = {}^{1}\!/_{\beta_{ao}} + {}^{1}\!/_{\beta_{ow}} \tag{2.13}$$

which is the same as $\sigma_{aw} = \sigma_{ao} + \sigma_{ow}$ ensures the *S-P* relations of air–water and air–LNAPL–water systems will match as an air–water system transitions into an air–LNAPL–water system and vice versa (Lenhard et al. 2002), which is important for convergence of numerical models as fluid systems change. Lenhard and Parker (1987a) noted that when measuring interfacial tensions, all fluids need to be in equilibrium with each other, particularly water. The condition given by Eq. (2.13) indicates that LNAPL will spread on water surfaces. A similar scaling approach was advanced by Leverett (1941) when he was extrapolating *S-P* data for one rock sample to similar rock types with different intrinsic permeabilities and porosities (slightly different pore structure between rock types) in petroleum reservoirs. Parker et al. (1987) extrapolated *S-P* data for different fluid systems in a porous medium with constant rigid pore structure —not between different porous media.

For nonhysteretic *k-S* relations, Parker et al. (1987) followed van Genuchten (1980) by employing the Mualem (1976) model for air–water systems, but extended it for air–LNAPL–water fluid systems in porous media to yield closed-form equations for predicting three-fluid relative permeabilities as

$$k_{rw} = \overline{S}_w^{0.5}\left\{1 - \left[1 - \overline{S}_w^{1/m}\right]^m\right\}^2 \tag{2.14}$$

$$k_{ro} = (\overline{S}_t - \overline{S}_w)^{0.5}\left\{\left[1 - \overline{S}_w^{1/m}\right]^m - \left[1 - \overline{S}_t^{1/m}\right]^m\right\}^2 \tag{2.15}$$

$$k_{ra} = \overline{S}_a^{0.5}\left(1 - \overline{S}_t^{1/m}\right)^{2m} \tag{2.16}$$

in which the k_{rw}, k_{ro}, and k_{ra} are the water, LNAPL, and air relative permeabilities, respectively, and m is a van Genuchten (1980) *S-P* parameter $\left(m = 1 - {}^1\!/_n\right)$. Closed-form expressions for relative permeabilities are in Parker and Lenhard (1989) when the Brooks-Corey (1966) *S-P* model is used in Burdine's (1953) relatively permeability integral.

The approach of Parker et al. (1987) allowed investigators to model air–water and air–LNAPL–water flow in the subsurface using numerical models that can be easily calibrated. Only air–water van Genuchten parameters α, n; the irreducible water saturation (S_m); and the interfacial tensions σ_{ao}, σ_{ow} are needed for the *k-S-P* relations when the van Genuchten (1980) and Mualem (1976) models are used for water-wet porous media. The nonhysteretic *k-S-P* relations were initially tested against air–LNAPL–water experimental data by Lenhard et al. (1988) in a multiphase numerical model. When the Brooks-Corey (1966) and Burdine (1953) models are used for water-wet porous media, only the air–water Brooks–Corey parameters h_d (displacement head) and λ (pore-size index); the irreducible water saturation (S_m); and the interfacial tensions σ_{ao}, σ_{ow} are needed for the *k-S-P* relations.

2.5 Hysteretic Model

Shortly after Parker et al. (1987) proposed the nonhysteretic *k-S-P* relations, Parker and Lenhard (1987) and Lenhard and Parker (1987b) proposed hysteretic *k-S-P* relations, which accounts for contact angle, pore geometry ("ink bottle"), and nonwetting fluid entrapment effects in the both vadose and liquid-saturated zones when fluids change from drying-to-wetting saturation paths and vice versa. The entrapment of LNAPL in water and entrapment of air in LNAPL and water are considered. Nonwetting fluid entrapment occupies pore space that would otherwise be occupied by a relative wetting fluid and displaces the relative wetting fluid into larger pore spaces. For example, entrapped LNAPL by water will displace water into larger pore spaces at the same actual water saturation and, thereby, increase the conductance rate of water. The effect increases the water relative permeability and decreases the LNAPL relative permeability at given actual water and LNAPL saturations for wetting fluid imbibition saturation paths than for wetting fluid drying saturation paths. To account for these effects, Parker and Lenhard (1987) and Lenhard and Parker (1987b) introduced the term "apparent" fluid saturations where the apparent two-phase (air–water)

water saturation is the sum of the effective entrapped air saturation in water and the effective water saturation; and the apparent three-phase (air–LNAPL–water) water saturation is the sum of the effective entrapped air and LNAPL saturations in water and the effective water saturation. The apparent saturations better index the pore sizes in which the continuous fluids reside than effective or actual saturations for predicting relative permeabilities. The hysteretic *k-S-P* relations were initially tested against transient air–LNAPL–water experimental data by Lenhard et al. (1995) in a multiphase numerical model, which yielded good results.

2.6 Predicting LNAPL Saturations, Volumes, and Transmissivity from Well Levels

To further help develop LNAPL remediation strategies and forecast three-dimensional LNAPL movement, Parker and Lenhard (1989) vertically integrated *k-S-P* relations and incorporated them into a two-dimensional numerical model (ARMOS) (Kaluarachchi et al. 1990). The earlier Parker et al. (1987) nonhysteretic *k-S-P* relations provided the framework. The model, ARMOS, was later modified to include LNAPL entrapment in both the unsaturated and liquid-saturated zones (Kaluarachchi and Parker 1992). The calculation of the LNAPL entrapment volume in a vertical slice of the unsaturated zone is based on the change in the air–LNAPL level in wells from rising water tables. The LNAPL entrapment volume in a vertical slice of the liquid-saturated zone is based on the change in the LNAPL–water level in wells from rising water tables. Parker et al. (1994) used ARMOS to model LNAPL migration and direct LNAPL recovery at LNAPL spill sites from knowledge of fluid levels in wells. Waddill and Parker (1997a) later proposed semi-analytical algorithms to predict LNAPL trapping and recovery from wells in diverse soils. The algorithms were incorporated in a version of ARMOS and tested against experimental data (Waddill and Parker, 1997b). Later, the approach of Parker and Lenhard (1989) was incorporated in American Petroleum Institute's (API) LDRM model (API 2007).

Parker and Lenhard (1989) developed the vertically integrated nonhysteretic *k-S-P* relations for incorporation into multiphase numerical models to assist remediation practitioners. However, not all LNAPL remediation practitioners have access to numerical models so Lenhard and Parker (1990) published equations for determining the LNAPL volume in a vertical slice of the subsurface from fluid level elevations in wells that can be used in simple computer programs. At the same time, Farr et al. (1990) also published equations to determine LNAPL volume in a vertical slice of the subsurface. Both publications assume vertical equilibrium conditions and use the Brooks-Corey (1966) *S-P* model for developing their equations. The difference in the approaches is Lenhard and Parker (1990) utilized elevations from the fluid levels in the wells to determine LNAPL and water pressures, and Farr et al. (1990) utilized depths from the surface to determine LNAPL and water pressures. The air phase is assumed to be atmospheric in both models.

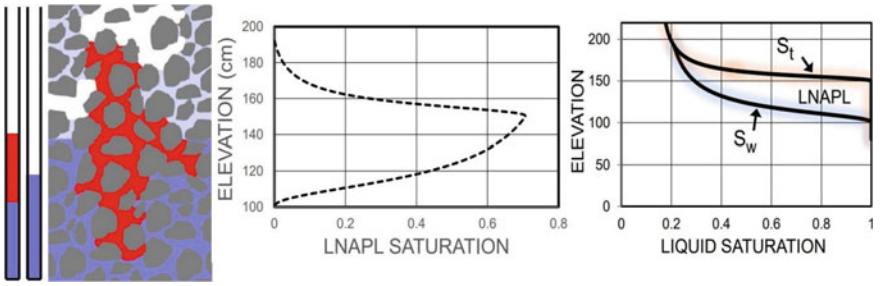

Fig. 2.1 A cartoon showing determining of total-liquid (S_t), water (S_w), and LNAPL saturations from wells adjacent to LNAPL-contaminated soils

Using the approach of Lenhard and Parker (1990) and Farr et al (1990) to determine LNAPL and water pressures, and hence air–LNAPL and LNAPL–water capillary pressures, from elevations (depths) of the air–LNAPL and LNAPL–water interfaces in the wells, the subsurface LNAPL saturations adjacent to wells can be calculated. Figure 2.1 shows an example of information that can be obtained. From the air–LNAPL and LNAPL–water capillary pressures, the total-liquid saturations (S_t) and the water saturations (S_w), respectively, can be calculated, which by difference yields the LNAPL saturations ($S_o = S_t - S_w$).

The shape of the Fig. 2.1 LNAPL saturation-elevation profile is similar to the "shark fin" shape description (Frollini and Petitta 2018) reported by researchers/practitioners. However, the shape depends on porous media type. For example, Fig. 2.2 shows the predicted LNAPL saturations as a function of elevation for the scenario where the air–LNAPL interface in a well is at an elevation of 150 cm above a datum and the LNAPL–water interface is at an elevation of 100 cm above the same datum for a LNAPL thickness in the well of 50 cm. If an accompanying well is only screened in the water-saturated zone, then the air–water interface would occur at an elevation of 135.5 cm above the datum, which can be determined from Eq. 2.5 in Lenhard and Parker (1990). Hydrostatic conditions are assumed so the LNAPL and water pressures vary linearly with elevation. Furthermore, nonhysteretic *S-P* relations are assumed, i.e., entrapped and residual LNAPL saturations are not considered. The datum elevation for determining the LNAPL saturations can be arbitrarily set. The predicted S_t and S_w, from which the LNAPL saturations are determined in Fig. 2.2, are obtained using the van Genuchten (1980) model, but other *S-P* models could be used (e.g., Brooks and Corey 1966; Alfaro Soto et al. 2019). The left diagram in Fig. 2.2 is for a loamy sand soil and the right diagram is for a clay loam soil. The shape of the predicted LNAPL saturation-elevation distribution is noticeably different, especially the LNAPL saturation values at each elevation. The LNAPL saturations in the clay loam soil extend to higher elevations than those in the loamy sand soil, but not to a large extent. The LNAPL saturations in Fig. 2.2 become zero at an elevation of 188 cm for the loamy sand soil and become zero at an elevation of 193 cm for the clay loam soil. The LNAPL saturation predictions in Figs. 2.1 and

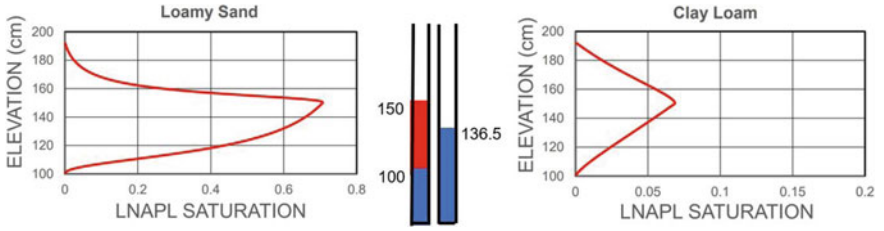

Fig. 2.2 Predicted LNAPL saturation-elevation distributions of a loamy sand (left) and a clay loam (right) soil for a scenario where the air–LNAPL interface in a well is at an elevation of 150 cm and the LNAPL–water interface is at 100 cm (center)

2.2 assumed that all the LNAPL is mobile or free as originally proposed by Lenhard and Parker (1990).

2.7 Incorporating Free, Residual, and Entrapped LNAPL Fractions

Later, Lenhard et al. (2004) proposed further adaptions to the *k-S-P* relations proposed by Parker et al (1987). Understanding that k_{ro} will be greater than 0 whenever the effective S_o ($\overline{S}_o$) is greater than 0, unless k_{ro} is arbitrarily set to zero at some $\overline{S}_o$, Lenhard et al. (2004) proposed an approach for methodically setting $k_{ro} = 0$ at variable S_o by considering a residual LNAPL saturation. When $k_{ro} > 0$ because $\overline{S}_o > 0$, then LNAPL will continually drain from the vadose zone until vertical *S-P* equilibrium conditions are established. Setting $k_{ro} = 0$ arbitrarily at some fixed S_o is not realistic because the mobility of LNAPL at different water saturations will not be the same. For example, setting $k_{ro}. = 0$ at $\overline{S}_o = 0.15$ might be reasonable when the effective water saturation ($\overline{S}_w$) = 0.2, because the LNAPL will reside in small pores; but, not when $\overline{S}_w = 0.7$, because the LNAPL will reside in larger pores. The LNAPL may be immobile when $\overline{S}_w = 0.2$, but much of the LNAPL will likely be mobile at $\overline{S}_w = 0.7$, so setting $k_{ro} = 0$ at some arbitrary LNAPL saturation is not reasonable for all water saturations.

Lenhard et al. (2004) considered LNAPL to exist in three forms: free, entrapped, and residual. Free LNAPL is continuous and can move freely in porous media when a LNAPL total-pressure gradient exists. Entrapped LNAPL is water-occluded LNAPL that results from water displacing LNAPL from pore spaces and can potentially exist everywhere in the subsurface (i.e., above and below the water-saturated zone). Entrapped LNAPL is discontinuous and immobile; it will not move under water and LNAPL total-pressure gradients typical in porous media. Residual LNAPL is immobile LNAPL that is not water occluded, which may exist as LNAPL wedges and films. There may be LNAPL films connecting some residual LNAPL (wedges) to free LNAPL, but the movement of LNAPL through the films is likely to be very slow and

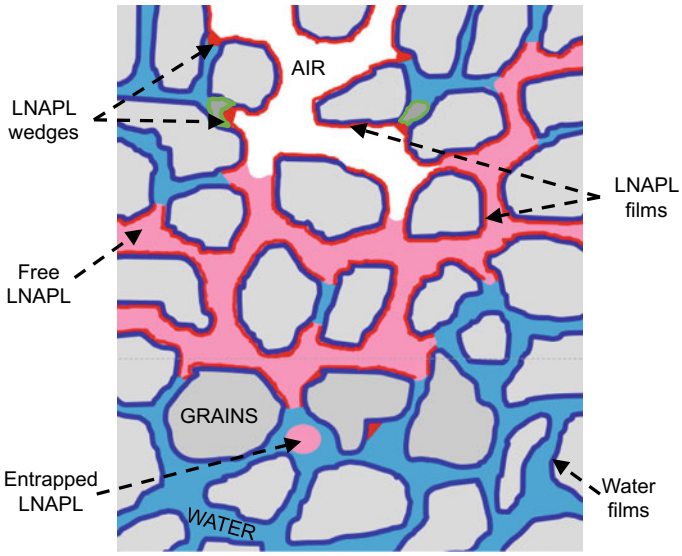

Fig. 2.3 A cartoon showing air (white), LNAPL (red), and water (blue) in subsurface pore spaces

cause the residual LNAPL to behave as if practically immobile under most LNAPL total-pressure gradients. Figure 2.3 shows a cartoon of air, LNAPL, and water in water-wet, subsurface, porous media as envisioned by Lenhard et al. (2004). Air is shown as white and exists when the air–LNAPL capillary pressure is greater than 0. LNAPL is shown as red with LNAPL films slightly darker red. The LNAPL films are attached to water films in pores containing air that previously were LNAPL filled and attached to water films in LNAPL-filled pores. Water-occupying pores is lighter blue. Water films wetting the solid particle grains (dark gray) is darker blue.

Figure 2.4 shows expanded sections of Fig. 2.3 which displays the Lenhard et al. (2004) concepts of free, entrapped, and residual LNAPL. Free LNAPL (Fig. 2.4a–c) is LNAPL continuous throughout the pore spaces that can move freely in response to LNAPL total-pressure gradients. It does not include LNAPL films (Fig. 2.4a,c) on water films (Fig. 2.4a,c) which theoretically will not move freely; the LNAPL films are assumed to be relatively immobile. Entrapped LNAPL (Fig. 2.4c) as explained earlier is water-occluded LNAPL which will not move in response to water and LNAPL total-pressure gradients. The water-occluded LNAPL is discontinuous and exists as blobs in pore bodies and LNAPL wedges that do not drain prior to water-filling pores during increasing water saturations. A similar situation may occur with water in smaller pores surrounded by larger pores that fill with LNAPL before the water in the small pores drain resulting in isolated water (Fig. 2.4b). Residual LNAPL is idealized as LNAPL wedges and films in the three-phase air–LNAPL–water zones (Fig. 2.4a). It also includes the relatively immobile LNAPL wedges and films (Fig. 2.4c) in the two-phase LNAPL–water zones.

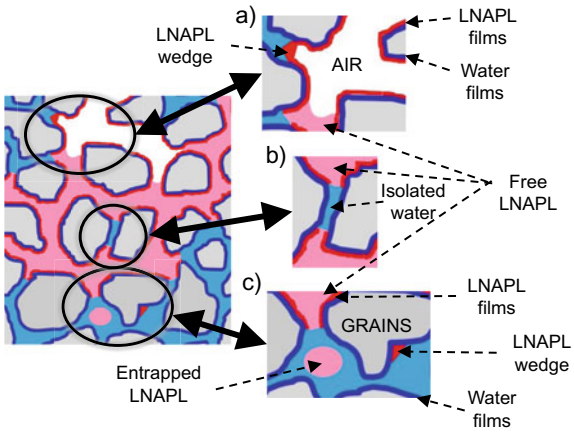

Fig. 2.4 A cartoon showing the concepts of free, entrapped, and residual LNAPL from Fig. 2.3

The concepts of free, entrapped, and residual LNAPL advanced by Lenhard et al. (2004) were incorporated in numerical codes by White et al. (2004) and Oostrom et al. (2005) and were shown to be important for predicting LNAPL behavior in the vadose zone. Additional models to incorporate a residual LNAPL saturation in *k-S-P* relationships were proposed by Wipfler and van der Zee (2001) and Van Geel and Roy (2002). Oostrom et al. (2005) tested both the Van Geel and Roy (2002) and Lenhard et al. (2004) formulations against transient three-fluid column experiments.

2.8 Recent Developments. The Lenhard et al. (2017) Model

Effects of entrapped and residual LNAPL (Lenhard et al. 2004) were considered by Lenhard et al. (2017) when predicting subsurface LNAPL saturations and transmissivity from LNAPL and water levels in wells. In the Lenhard et al. (2017) model, historical air–LNAPL and LNAPL–water interface levels in wells were considered. Specially, the highest air–LNAPL interface elevation and the lowest LNAPL–water interface elevation were included. The highest air–LNAPL interface elevation in an observation well reflects the highest elevations in the subsurface that may contain residual LNAPL. The lowest LNAPL–water interface elevation reflects the lowest elevations that may contain entrapped LNAPL. Both entrapped and residual LNAPL will affect the LNAPL relative permeability at a location because they reduce the amount of free or mobile LNAPL at that elevation. The LNAPL relative permeability distribution governs the LNAPL transmissivity.

For the same configuration of air–LNAPL and LNAPL–water interface elevations in a well as Fig. 2.2 (current levels) and assuming the air–LNAPL interface elevation at one time was 50 cm higher (i.e., historical elevation is 200 cm) and the LNAPL–water interface elevation was 50 cm lower (i.e., historical elevation is 50 cm), predicted free, entrapped, and residual LNAPL saturations are shown in

Fig. 2.5. Again, the van Genuchten (1980) model was used to predict the *S-P* relations consistent with the Lenhard et al. (2017) model. In comparison to Fig. 2.2, the upper free LNAPL elevation for the loamy sand soil in Fig. 2.5 is predicted to be about 20 cm lower. This results because residual LNAPL occurs, which is not mobile (free), and some minor entrapped LNAPL exists as water displaced LNAPL from those pores when the water table was raised (i.e., as the LNAPL–water interface in the well was raised from the historical level). The residual LNAPL for the loamy sand soil in Fig. 2.5 is predicted to occur about 50 cm higher than the free LNAPL in Fig. 2.2, because the historical air–NAPL level is 50 cm higher. The lower free LNAPL elevation is the same for the loamy sand soil in Figs. 2.2 and 2.5 because the lower free LNAPL occurrence is a function of the current LNAPL–water level (i.e., 100-cm elevation) and not historical levels. However, the lower entrapped LNAPL elevation for the loamy sand soil in Fig. 2.5 is predicted to be about 50 cm lower than the free LNAPL in Fig. 2.2 because the historical LNAPL–water level is 50 cm lower. There is no predicted entrapped LNAPL in Fig. 2.2 because it was not considered in the nonhysteretic *S-P* relations. For Fig. 2.5, the maximum possible entrapped LNAPL was set at 0.15, and the maximum possible residual LNAPL was set at 0.15. These are additional parameters in Lenhard et al. (2004, 2017). The LNAPL distributions in Fig. 2.5 can help practitioners design remediation programs focused on free, entrapped, and residual LNAPL and not only on free LNAPL as in Fig. 2.2.

The predicted free LNAPL volume in a vertical slice of the loamy sand soil per cm^2 of surface area in Fig. 2.2 is predicted to be 11.7 cm^3/cm^2, whereas the free LNAPL volume is predicted only to be 9.9 cm^3/cm^2 in Fig. 2.5. The difference is because of considering residual and entrapped LNAPL in Fig. 2.5. The difference also has a significant effect on predicted LNAPL transmissivities using the methodology in Lenhard et al. (2017). When entrapped and residual LNAPL are not considered, the predicted free LNAPL transmissivity is 6200 cm^2/day for the loamy sand soil with an assumed water-saturated hydraulic conductivity of 350 cm/day. When entrapped and residual LNAPL are considered, the predicted free LNAPL transmissivity is 4225 cm^2/day—a difference of over 30%. If a calculation is conducted that accounts for only LNAPL under positive LNAPL pressures, then the predicted free LNAPL

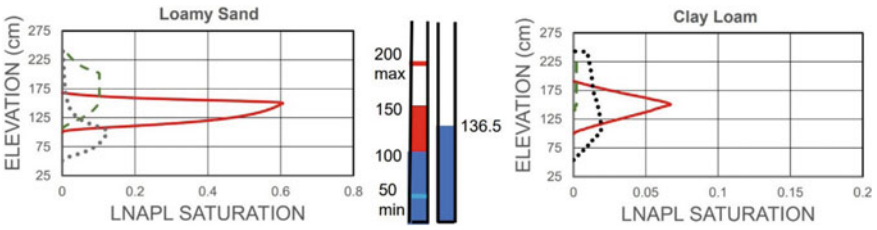

Fig. 2.5 Predicted free (red solid line), entrapped (black dotted line), and residual (green dashed line) of a loamy sand (left) and a clay loam (right) soil where the current air–LNAPL and LNAPL–water interface elevations in a well are the same as in Fig. 2.2 with the historical highest air–LNAPL level 50 cm higher than current and the historical lowest LNAPL–water level 50 cm lower than current

transmissivity is only 4830 cm^2/day for the loamy sand in Fig. 2.2 and 3360 cm^2/day in Fig. 2.5. Because only LNAPL under positive pressure will enter a borehole, estimations of LNAPL transmissivity should be based on LNAPL under positive pressure for planning direct LNAPL recovery from wells.

2.9 Layered Porous Media

When the contaminated subsurface can be represented as homogeneous, the subsurface LNAPL distributions can have a "shark fin" shape. For layered porous media, however, the subsurface LNAPL distribution shape can be more varied. Consider a scenario where two coarse layers are separated by a fine layer. Assume a LNAPL-contaminated subsurface with a 20-cm fine layer between two coarse layers that may be over 100 cm thick. In nearby monitoring wells, the air–LNAPL interface in one well occurs at an elevation of 160 cm above the datum and the LNAPL–water interface in the same well occurs at an elevation of 100 cm above the datum for a LNAPL thickness of 60 cm in the well. In an accompanying well screened only in the water-saturated zone, the air–water interface occurs at an elevation of 142 cm above the datum. Assuming hydrostatic conditions, nonhysteretic *S-P* relations, and the van Genuchten (1980) model to predict S_t and S_w, the subsurface LNAPL saturation distribution can be predicted. Figure 2.6 shows the results for the fine layer occurring between the 120- and 140-cm elevations. Because the fine layer is below the air–LNAPL interface in the well and above the elevation of the LNAPL–water interface, the fine layer will be completely saturated with LNAPL and water. The fine layer will have a higher water saturation than the coarse layers because of its smaller pore sizes. The contrast in pore sizes between the coarse and fine layers can produce significant differences in LNAPL saturations at the boundaries between the layers. The resulting shape of the subsurface LNAPL distribution will consequently be very different than a "shark fin" shape.

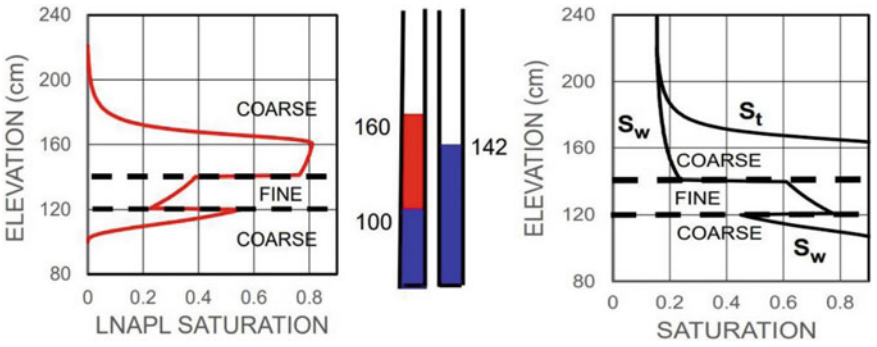

Fig. 2.6 Predicted LNAPL, total-liquid (S_t), and water (S_w) saturations for a scenario involving a fine layer between two coarse layers with 60 cm of LNAPL inside a nearby monitoring well

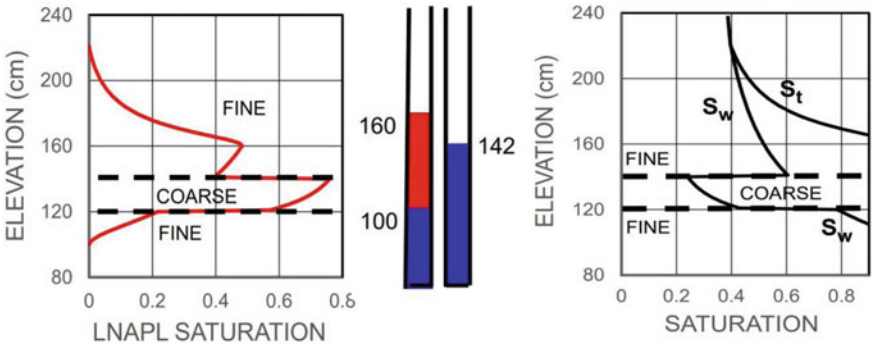

Fig. 2.7 Predicted LNAPL, total-liquid (S_t), and water (S_w) saturations for a scenario involving a coarse layer between two fine layers with 60 cm of LNAPL inside a nearby monitoring well

The shape of the subsurface LNAPL distribution curve will depend on whether there are contrasting pore sizes between potential layers, the location of the layers relative to the air–LNAPL and LNAPL–water interface elevations in nearby wells, and the thickness of LNAPL in the wells. As another example, consider a scenario where two fine layers are separated by a coarse layer. Assume a LNAPL-contaminated subsurface with a 20-cm coarse layer between two fine layers that may be over 100 cm thick. The opposite configuration as for Fig. 2.6. Further, assume the same conditions and fluid levels in wells as for Fig. 2.6. Using the same calculation protocols, Fig. 2.7 shows the results of the predicted total liquid, S_t, and water, S_w, saturations. For Fig. 2.7, the coarse layer is completely liquid-saturated for the same reason as the fine layer in Fig. 2.6, but the water saturation is low because of its larger pore sizes. The low water saturation yields a high LNAPL saturation for the coarse layer. The contrasting sizes of pores in the coarse and fine layers produce a significant difference in LNAPL saturations at the boundaries of the layers—just like in Fig. 2.6, but in the opposite direction. The shape of the subsurface LNAPL distribution curve can be quite complex for layered porous media and not a simple "shark fin" shape. Furthermore, an abrupt change in pore sizes at layer boundaries can result in LNAPL moving laterally versus downward similarly to a capillary break of constructed soil covers over waste pits. The subsurface LNAPL distribution depends on many factors.

2.10 Summary and Steps Forward

The historical development of *k*-*S*-*P* relations described in this chapter largely follows advancements proposed by Parker, Lenhard, and colleagues. Many of their proposed concepts and equations are incorporated in today's multiphase numerical models or code developers have used some of their concepts in building their models. However, further advancements are still required to help accurately predict the subsurface

behavior of LNAPL, especially the effects of microbiological action and potential changes in fluid properties over time.

A key element of *k-S-P* models is that they mimic physics of multiphase flow, even if the models may be empirical. The various forms of LNAPL in the subsurface need to be addressed. Careful estimation of model parameters is needed also to produce good predictions, but this is not routinely done by contaminated land practitioners nor typically required by regulators. Improved and more accessible measurement methods for two-fluid and three-fluid systems should be developed and adopted.

Similarly, the effects of heterogeneous subsurface conditions should be acknowledged by investigators and considered when conducting numerical simulations or using simple predictive models. This may be incorporated into models specifically developed to represent heterogeneous environments with layered systems or multimodal pore-size porous media (see Chap. 3).

Some models to predict LNAPL volumes, distribution, and transmissivity may not account for certain processes, which may have not been considered relevant enough for practical purposes in the past. Additional research may be needed to elucidate the relevance of mechanisms like those associated to natural source zone depletion (e.g., entrapment of gases caused by methanogenic outgassing or presence of microorganisms and extracellular polymeric substances) on LNAPL distribution predictions. More information on natural source; zone depletion phenomena is presented in Chap. 5. Further research is also needed for systems not exhibiting strongly water-wet characteristics.

Good understanding of multiphase flow principles is paramount to develop sound conceptual site models and, therefore, should be an essential skill of regulators and practitioners managing LNAPL-contaminated sites. Multiphase models are currently underutilized and may help to analyze LNAPL remediation options and design cost-effective solutions, including mass recovery systems (see Chap. 12) and any other in-situ remediation strategies targeting the LNAPL source zone.

References

Abriola LM, Pinder GF (1985a) A multiphase approach to the modeling of porous media contamination by organic compounds-part I: equation development. Water Resour Res 21(1):11–18

Abriola LM, Pinder GF (1985b) A multiphase approach to the modeling of porous media contamination by organic compounds-part 2: numerical simulation. Water Resour Res 21(1):19–26

Anderson WG (1987) Wettability literature survey - Part 4: effects of wettability on capillary pressure. J Pet Technol 39:1283–1300. https://doi.org/10.2118/15271-PA

API (American Petroleum Institute) (2007) Volume 1: distribution and recovery of petroleum hydrocarbon liquids in porous media. API Publication 4760. Washington D.C, pp 53

ATSDR (Agency for Toxic Substances and Disease Registry) (1995) Toxicological profile for gasoline. U.S. Department of Health and Human Services. Division of Toxicology/Toxicology Information Branch 1600 Clifton Road NE, E-29. https://www.atsdr.cdc.gov/toxprofiles/tp72.pdf

Baehr AL, Corapcioglu MY (1987) A compositional multiphase model for groundwater contamination by petroleum products, 2 numerical solution. Water Resour Res 23:201–213

Brooks RH, Corey AT (1966) Properties of porous media affecting fluid flow. J Irrig Drain Div Am Soc Civ Eng 92:61–68
Burdine HT (1953) Relative permeability calculations from pore-size distribution data. Trans Soc Pet Eng AIME 198:71–77
de Pastrovich TL, Baradat Y, Barthel R, Chiarelli A, Fussell DR (1979) Protection of groundwater from oil pollution. CONCAWE, Report 3/79. Den Haag, Netherlands, pp 61
EPA (U.S. Environmental Protection Agency) (2007) Agency for toxic substances and disease registry (ATSDR), August 2007. Toxicological Profile for Benzene. https://www.epa.gov/sites/default/files/2014-03/documents/benzene_toxicological_profile_tp3_3v.pdf
Farr AM, Houghtalen RJ, McWhorter DB (1990) Volume estimation of light nonaqueous phase liquids in porous media. Ground Water 28(1):48–56
Faust CR (1985) Transport of immiscible fluids within and below the unsaturated zone: a numerical model. Water Resour Res 21:587–596
Frollini E, Petitta M (2018) Free LNAPL volume estimation by pancake model and vertical equilibrium model: comparison of results, limitations, and critical points. Geofluids, Article ID 8234167:13. https://doi.org/10.1155/2018/8234167
Hall RA, Blake SB, Champlin SCJ (1984) Determination of hydrocarbon thicknesses in sediments using borehole data. In: Proceedings of the fourth national symposium on aquifer restoration and ground water monitoring. National Water Well Assoc., Worrthington, OH, pp 300–304
Hampton DR, Miller PDG (1988) Laboratory investigation of the relationship between actual and apparent product thickness in sands. In: Proceedings petroleum hydrocarbons and organic chemicals in ground water: prevention, detection and restoration. National Water Well Assoc., Dublin, OH, pp 157–181
Hassanizadeh SM, Gray WG (1990) Mechanics and thermodynamics of multiphase flow in porous media including interphase boundaries. Adv Water Resour 13(4):169–186
IARC (International Agency for Research and Cancer) (1987) Summaries and evaluations: Benzene (Group 1). Lyon, International Agency for Research on Cancer, p 120 (IARC Monographs on the Carcinogenicity of Chemicals to Humans, Supplement 7. http://www.inchem.org/documents/iarc/suppl7/benzene.html
Kaluarachchi JJ, Parker JC (1989) Improving the efficiency of finite element method in modeling multiphase flow. Water Resour Res 25:43–54
Kaluarachchi JJ, Parker JC (1992) Multiphase flow in porous media with a simplified model for oil entrapment. Trans Porous Media 7:1–13
Kaluarachchi JJ, Parker JC, Lenhard RJ (1990) A numerical model for areal migration of water and light hydrocarbon in unconfined aquifers. Ad Water Resour. 13(1):29–40
Kuppusamy T, Sheng J, Parker JC, Lenhard RJ (1987) Finite element analysis of multiphase immiscible flow through soils. Water Resour Res 23:625–631
Lenhard RJ, Parker JC (1987a) Measurement and prediction of saturation-pressure relationships in three-phase porous media systems. J Contam Hydrol 1:407–424
Lenhard RJ, Parker JC (1987b) A model for hysteretic constitutive relations governing multiphase flow: 2 permeability-saturation relations. Water Resour Res 23:2197–2206
Lenhard RJ, Parker JC (1990) Estimation of free hydrocarbon volume for fluid levels in monitoring wells. Ground Water 28(1):57–67
Lenhard RJ, Oostrom M, White MD (1995) Modeling fluid flow and transport in variably saturated porous media with the STOMP simulator. 2. Verification and validation exercises. Adv Water Resour 18(6):365–373
Lenhard RJ, Oostrom M, Dane JH (2002) Chapter 7.5: prediction of capillary pressure-relative permeability relations. In: Methods of soil analysis. Part 1: physical methods. In: Dane JH and Topp GC (eds) Soil Science of America. Madison, WI. pp 1591–1607
Lenhard RJ, Oostrom M, Dane JH (2004) A constitutive model for air-NAPL-water flow in the vadose zone accounting for immobile, non-occluded (residual) NAPL in strongly water-wet porous media. J Contam Hydrol 73:283–304

Lenhard RJ, Rayner JL, Davis GB (2017) A practical tool for estimating subsurface LNAPL distributions and transmissivity using current and historical fluid levels in groundwater wells: effects of entrapped and residual LNAPL. J Contam Hydrol 205:1–11

Lenhard RJ, Dane JH, Parker JC, Kaluarachchi JJ (1988) Measurement and simulation of one-dimensional transient three-phase flow for monotonic liquid drainage. Water Resour Res 24:853–863

Leverett MC (1941) Capillary behavior in porous solids. Trans Soc Pet Eng AIME 142:152–169

Lewis J (1985) Lead poisoning: a historical perspective. EPA J 11(4):15–18. (U.S. Environmental Protection Agency) https://archive.epa.gov/epa/aboutepa/lead-poisoning-historical-perspective.html

Mualem Y (1976) A new model for predicting the hydraulic conductivity of unsaturated porous media. Water Resour Res 12:513–522

Osborne M, Sykes JF (1986) Numerical modeling of immiscible organic transport at the Hyde Park landfill. Water Resour Res 22:25–33

Oostrom M, White MD, Lenhard RJ, Van Geel J, Wietsma TW (2005) A comparison of models describing residual NAPL formation in the vadose zone. Vadose Zone J 4:163–174

Oudijk G (2007) The use of alkyl leads in gasoline age-dating investigations: new insights, common investigative techniques, limitations, and recommended practices. Environ Claims J 19(1–2):68–87. https://doi.org/10.1080/10406020601158329

Parker JC, Lenhard RJ (1987) A model for hysteretic constitutive relations governing multiphase flow: 1 saturation-pressure relations. Water Resour Res 23:2187–2196

Parker JC, Lenhard RJ (1989) Vertical integration of three-phase flow equations for analysis of light hydrocarbon plume movement. Trans Porous Media 5:187–206

Parker JC, Lenhard RJ, Kuppusamy T (1987) A parametric model for constitutive properties governing multiphase flow in porous media. Water Resour Res 23(4):618–624

Parker JC, Zhu JL, Johnson TG, Kremesec VJ, Hockman EL (1994) Modeling free product migration and recovery at hydrocarbon spill sites. Ground Water 32(1):119–128

Richards LA (1931) Capillary conduction of liquids through porous mediums. Physics 1:318–333. https://doi.org/10.1063/1.1745010

Schwille F (1967) Petroleum contamination of the subsoil—a hydrological problem. In: Hepple P (ed) The joint problems of the oil and water industries. Inst. Petrol, London, pp 23–54

Soto MAA, Lenhard R, Chang HK, van Genuchten MT (2019) Determination of specific LNAPL volumes in soils having a multimodal pore-size distribution. J Environ Mgt 237:576–584

van Dam J (1967) The migration of hydrocarbons in water-bearing stratum. In: Hepple P (ed) The joint problems of the oil and water industries. Inst. Petrol, London, pp 55–96

Van Geel PJ, Roy SD (2002) A proposed model to include residual NAPL saturation in a hysteretic capillary pressure-saturation relationship. J Contam Hydrol 58:79–110

van Genuchten MT (1980) A closed-form equation for predicting the hydraulic conductivity of unsaturated soils. Soil Sci Soc Am J 44:892–898 https://doi.org/10.2136/sssaj1980.03615995004400050002x

Waddill DW, Parker JC (1997a) A semianalytical model or predict recovery of light, nonaqueous phase liquids from unconfined aquifers. Ground Water 35(2):280–290

Waddill DW, Parker JC (1997b) Recovery of light, non-aqueous phase liquid from porous media: laboratory experiments and model validation. J Contam Hydrol 27:127–155

White MD, Oostrom M, Lenhard RJ (2004) A practical model for mobile, residual, and entrapped NAPL in water-wet porous media. Ground Water 42(5):734–746

Wipfler EL, van der Zee SEATM (2001) A set of constitutive relationships accounting for residual NAPL in the unsaturated zone. J Contam Hydrol 50:53–77